Full Paper
doi.org/10.1002/chem.202001416

Host–Guest Chemistry

Redox-Active Supramolecular Heteroleptic $M_4L_2L'_2$ Assemblies with Tunable Interior Binding Site

Raoul Plessius,[a] Vera Deij,[a] Joost N. H. Reek,*[a] and Jarl Ivar van der Vlugt*[a, b]

Abstract: Three $Pt_4L_2L'_2$ heteroleptic rectangles (**1**–**3**), containing ditopic redox-active bis-pyridine functionalized perylene bisimide (PBI) ligands **PBI-pyr$_2$** (**L**) are reported. Co-ligand **L′** is a dicarboxylate spacer of varying length, leading to modified overall size of the assemblies. ^{1}H NMR spectroscopy reveals a trend in the splitting and upfield chemical shift of the PBI-hydrogens in the rectangles with respect to free PBI, most pronounced with the largest strut length (**3**) and least with the smallest strut length (**1**). This is attributed to increased rotational freedom of the **PBI-pyr$_2$** ligand over its longitudinal axis (N_{py}-N_{py}), due to increased distance between the PBI-surfaces, which is corroborated by VT-NMR measurements and DFT calculations. The intramolecular motion entails desymmetrization of the two PBI-ligands, in line with cyclic voltammetry (CV) data. The first (overall two-electron) reduction event and re-oxidation for **1** display a subtle peak-to-peak splitting of 60 mV, whilst increased splitting of this event is observed for **2** and **3**. The binding of pyrene in **1** is probed to establish proof of concept of host-guest chemistry enabled by the two PBI-motifs. Fitting the binding curve obtained by ^{1}H NMR titration with a 1:1 complex formation model led to a binding constant of $964 \pm 55\ M^{-1}$. Pyrene binding is shown to directly influence the redox-chemistry of **1**, resulting in a cathodic and anodic shift of approximately 46 mV on the first and second reduction event, respectively.

Introduction

Coordination chemistry provides tools for the construction of well-defined multinuclear architectures that offer functionality by means of their shape, that is, the presence of some sort of cavity that may be used to encapsulate a guest molecule. The simplest of these are two-dimensional multinuclear species that form Euclidian geometries, such as triangles, squares and related shapes. Over the last decades, numerous M_4L_4 metallosquares have been synthesized. There are examples of homoleptic squares using a single ditopic ligand based on porphyrin,[1] perylene bisimide[2] or 4,4′-bipyridine frameworks.[3–5] By using two different ligands in a single assembly, heteroleptic $M_4L_2L'_2$ analogues are accessible that offer more control over the dimensions of the molecular assemblies.[6–10] To date, supramolecular interactions and host-guest chemistry with 2D architectures is relatively limited in comparison to 3D-analogues. This is particularly true for heteroleptic versions of these molecular assemblies, despite their relative ease of synthesis compared to 3D-derivatives that contain more than one type of organic strut. Furthermore, heteroleptic derivatives in principle allow for more precise tuning of the inner cavity space by varying the length of the second organic strut (Scheme 1).

The incorporation of redox-active components into self-assembled assemblies has recently received attention, as it provides an entry to control chemical events[11] and may be relevant for sensing applications.[12] We recently demonstrated how the integration of two different types of redox-active ligands enables the reversible storage of up to 16 electrons in a Fujita-type 3D supramolecular assembly.[13] The dimensions

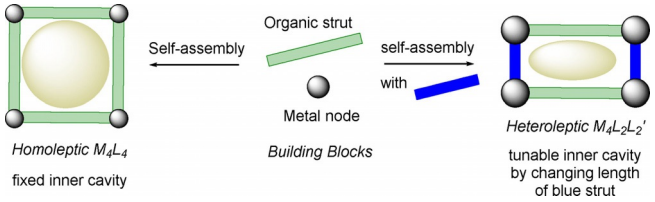

Scheme 1. Formation of homo- and heteroleptic supramolecular 2D assemblies, with the latter allowing for facile tuning of the inner cavity space by manipulation of length of the blue strut.

[a] *R. Plessius, V. Deij, Prof. Dr. J. N. H. Reek, Prof. Dr. Ir. J. I. van der Vlugt*
van't Hoff Institute for Molecular Sciences (HIMS)
University of Amsterdam (UvA)
Science Park 904, 1098 XH Amsterdam (The Netherlands)
E-mail: j.n.h.reek@uva.nl
j.i.vandervlugt@uva.nl

[b] *Prof. Dr. Ir. J. I. van der Vlugt*
Current address:
Institute of Chemistry
Carl von Ossietzky University Oldenburg
Carl-von-Ossietzky-Strasse 9–11, 26129 Oldenburg (Germany)
E-mail: jarl.ivar.van.der.vlugt@uni-oldenburg.de

Supporting information and the ORCID identification number(s) for the author(s) of this article can be found under:
https://doi.org/10.1002/chem.202001416.

and geometry of these cages led to completely independent switching of the three redox-events. However, in light of potential sensing or separation applications, it can be of interest to develop systems wherein redox-events are not independent and thus may be influenced and tuned in subtle ways, for instance by guest encapsulation. Such an arrangement is more easily realized in stimulus-responsive 2D-architectures, opening up the possibility of combining (known) photophysical or electrochemical properties with encapsulation behaviour, particularly in the context of installing redox-responsive motifs. This requires access to an easily variable and versatile platform, understanding of the ensuing intramolecular as well as host-guest interactions and of the potential influence of size on the response upon applying an external stimulus.

The redox-activity of perylene bisimides (PBIs) is well-established,[14] with two reversible one-electron reduction events localized at the central conjugated aromatic unit within these systems. The motif is amenable to versatile functionalization at for instance the N-termini,[15] which makes it an interesting building block for use in macrocyclic and supramolecular chemistry, also because (non-)covalent linkages are relatively remote from the redox-site. The group of Würthner has demonstrated the formation of covalent cyclophanes and related macrocycles bearing two linked PBI units and has explored the host-guest chemistry and photochemistry of these assemblies. Furthermore, coordination of pyridine-appended PBIs to Pt^{II} afforded a homoleptic molecular square that retained its PBI-centered fluorescent and electroactive properties upon assembly.[16,17] They also proposed a staggered orientation of both aromatic fragments to be the thermodynamically most favourable conformation, which would allow the two PBI-fragments to undergo a "flipping" motion. This was supported by variable temperature NMR (VT NMR) data, showing coalescence of the PBI-hydrogen signals at *high temperature* as a result of rapid motion of the square. Only one example of self-assembly of a heteroleptic PBI-containing molecular assembly exists, to the best of our knowledge.[18] Strikingly, the potential interplay between host-guest chemistry properties and built-in redox-responsive character of molecular squares is relatively unexplored to date.[12a,h]

Herein, we show the synthesis and electrochemistry of heteroleptic $\mathbf{M_4L_2L'_2}$-type molecular rectangles bearing redox-active PBI-based ditopic pyridyl linkers (**L**). Tunable mutual proximity of these redox-loci, by virtue of the variable dicarboxylate (**L′**) strut length, creates a binding pocket for planar aromatic molecules via π–π interactions (Scheme 2).[19] Moreover, the strut length influences the redox-properties of empty molecular squares, as a result of rotational motion of the PBI-based struts. We also report on the electrochemical response of the supramolecular assembly in the presence of guest.

Results and Discussion

Synthesis of empty heteroleptic molecular rectangles 1–3 and binding of pyrene

The redox-active linker **PBI-Pyr$_2$** was prepared in five steps from commercially available starting materials, using a reported method.[20] Heteroleptic assemblies **1**–**3** were assembled using three different dicarboxylate spacers—terephthalate (**tp**), 2,6-naphthalenedicarboxylate (**np**) and biphenyl-4,4′-dicarboxylate (**bp**) (Scheme 3). Reaction of **PBI-Pyr$_2$**, the sodium salt of the respective dicarboxylate spacer and *cis*-$[Pt(PEt_3)_2(OTf)_2]$ in a H_2O/acetone (1:4) mixture for 4 hours at 75 °C and subsequent work-up produced the desired complexes as microcrystalline red solids that were fully characterized using multinuclear NMR spectroscopy and high resolution mass spectrometry. Literature suggests that heteroleptic complex formation may be fav-

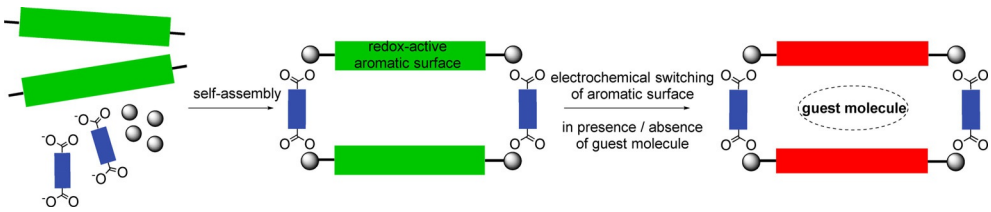

Scheme 2. Electrochemical switching of redox-active ligand **PBI-Pyr$_2$** (green bar) in heteroleptic $\mathbf{M_4L_2L'_2}$ assemblies in presence/absence of a suitable guest molecule.

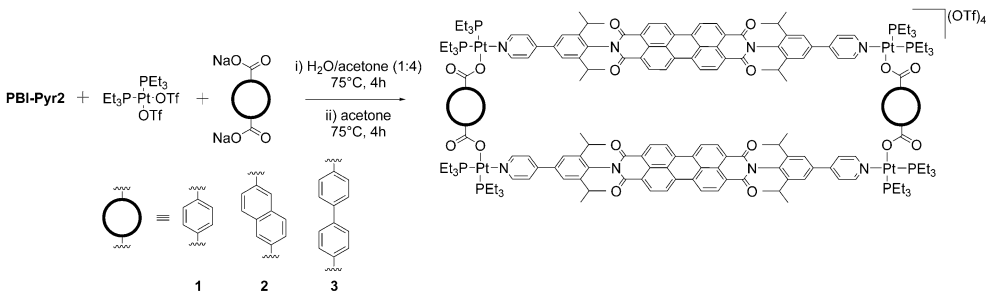

Scheme 3. Multi-component synthesis of heteroleptic $M_4L_2L'_2$ rectangles **1**–**3**.

oured over the production of a homoleptic complex because of a charge separation effect of the negative carboxylate and the neutral pyridyl.[21] The well-defined intramolecular PBI-PBI distance in these assemblies is 6.9 (**tp**), 9.1 (**np**) and 11.3 Å (**bp**), respectively, based on molecular modelling (Figure 1), supporting the tunable character of the pocket in this series of complexes.

All three assemblies displayed similar ^{31}P NMR spectra, containing two doublets (δ 7.08 and 1.46 ppm in CD_2Cl_2, $J_{P\text{-}P}$ = 21.7 Hz for **1**, see Supporting Information for **2** and **3**), as well as weak ^{195}Pt-satellites accompanying each signal ($^1J_{Pt\text{-}P}$ = 3254 and 3445 Hz for **1**). These data support the heteroleptic coordination mode to platinum expected for an $\mathbf{M_4L_2L'_2}$ composition, with mutual *cis*-orientation of the two PEt_3 ligands and the more upfield signal assigned to the PEt_3 ligand *trans* to pyridine.[22] Furthermore, HR-MS confirmed the elemental composition for all complexes with no indication for any homoleptic complex formation. UV/Vis absorption spectra of **1** in CH_2Cl_2 displayed characteristic PBI absorption features with λ_{max} at 528, 490 and 461 nm.[23] Fluorescence spectroscopy (see the Supporting Information) confirmed that the fluorescence of the ligand is not quenched upon assembly.

To establish proof of concept capability of the binding pocket defined by the two PBI-motifs for host-guest interactions, the binding of the small flat aromatic guest pyrene inside **1** was probed. Mixing **1** and 1 equivalent of pyrene in CD_3CN results in upfield shifting of the PBI-hydrogens in the ^{1}H NMR spectrum by 0.16 and 0.05 ppm with respect to the empty rectangle. The signals of the guest are shifted upfield (see Figure S19). From a ^{1}H NMR titration at a constant host concentration ([**1**] = 0.25 mM) with up to 60 equiv of pyrene in CD_3CN, a binding constant of 964 ± 55 M^{-1} was established. ^{1}H NMR DOSY spectroscopy on a 1:1 mixture of **1** and pyrene at 0.25 mM in [D_3]acetonitrile showed that on average only a part of the pyrene is bound in the cage, in line with the relatively low concentration and the measured binding constant (Figure S20). A titration experiment with pyrene as guest using the larger assembly **3** as host showed a low binding constant of 48 ± 2 M^{-1}. Most likely the large PBI-PBI distance in this assembly prevents simultaneous interactions of the pyrene guest with both aromatic surfaces.

Dynamics of empty heteroleptic molecular rectangles 1–3—NMR spectroscopy

The ^{1}H NMR spectra for free **1**–**3** reveal the expected downfield shifts for the pyridyl hydrogens in all three assemblies, resulting from coordination to the Pt^{II} cornerstones. Only minor electronic changes were anticipated for the remaining hydrogens within the ligand framework upon complex formation, given the distance from the Pt^{II} coordination site, and most signals indeed show only minor shifts. However, the aromatic PBI-hydrogens shift rather differently in the three heteroleptic species. For the smallest rectangle **1** the two doublets attributed to the PBI backbone are found at δ 8.79 and 8.67 ppm, whereas for the largest rectangle **3** these signals shift upfield to δ 8.47 and 8.13 ppm, respectively ($\Delta\delta$ 0.32 and 0.54 ppm compared to **1**, Figure 2). Moreover, the signals do not only shift upfield, but the signals of these aromatic hydrogen atoms shift relative to each other. In the free ligand, these PBI-hydrogens overlap to form a quasi-singlet ($\Delta\delta$ 0 ppm), while for **1** the splitting between the two doublets is $\Delta\delta$ 0.12 ppm and for **3** the splitting is almost three times larger ($\Delta\delta$ 0.34 ppm). Similar shifts are observed for the naphthalene-based rectangle, fol-

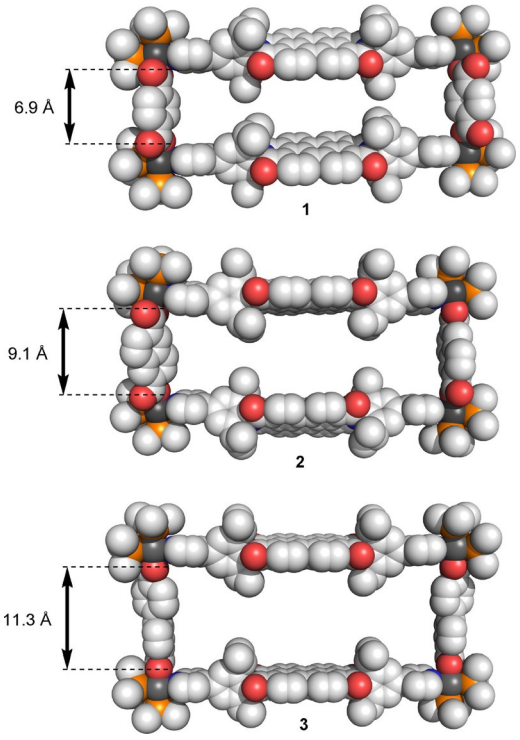

Figure 1. 3D modelled structures of **1**–**3** highlighting the intrinsic spacer length (O–O distance) of the **tp**, **np** and **bp** linkers as measure for intramolecular PBI-PBI distance.

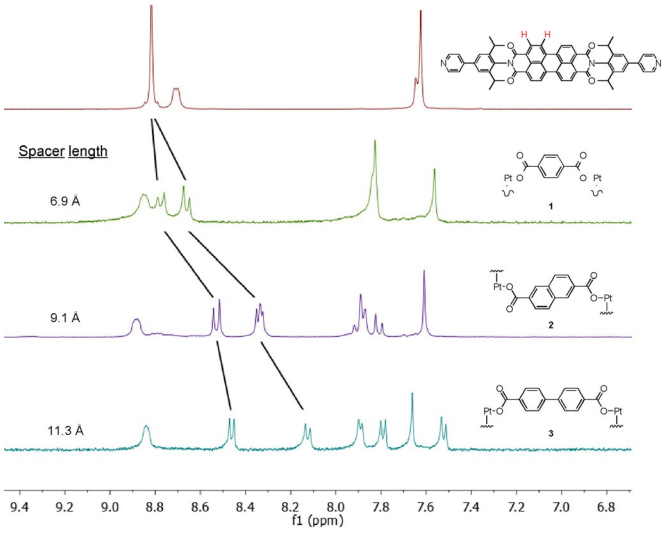

Figure 2. ^{1}H NMR zoom of the aromatic region of (top to bottom) free **PBI-Pyr$_2$** and rectangles **1**–**3** in CD_2Cl_2, demonstrating splitting and upfield shifting of the PBI-hydrogen signals as a function of dicarboxylate spacer length.

lowing the trend and falling in-between the terephthalate- and biphenyl-based rectangles in terms of chemical shifts.

The observed shifts of these aromatic signals in the ^{1}H NMR spectra with increasing dicarboxylate spacer length are hypothesized to relate to increased rotational freedom of the PBI fragments. This could manifest itself in either one of the following two dynamic movements: i) The supramolecular assembly either exhibits "flipping" between two different staggered conformations (Figure 3, top), analogous to the system described by Würthner,[24] or ii) the **PBI-pyr$_2$** ligand rotates along its longitudinal axis (N_{py}-N_{py} axis). In the latter case, the two aromatic PBI hydrogens H_{inner} and H_{outer} each experience a different ring current shift due to the neighbouring aromatic system, explaining the respective upfield shifting of both signals. Calculations suggest that for **1** a mutual parallel orientation is most preferred. The proximity of the two PBI systems in rectangle **1** virtually prevents rotation of one unit relative to the other (Figure 3, bottom). In complex **3**, the increased distance between both PBI fragments creates a larger pocket that results in more rotational freedom of the **PBI** unit, in line with the larger shifts observed in the NMR spectrum.

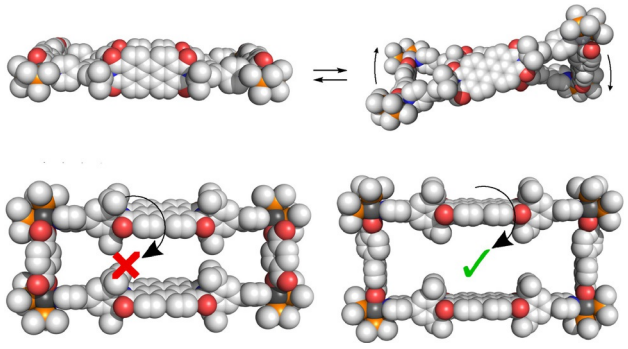

Figure 3. Top: "flipping" of the two PBI-systems from a parallel orientation (left) to a staggered conformation (right). Bottom: 3D modelled structures of **1** (left) and **3** (right) to emphasize difference in rotational freedom along the longitudinal N_{py}–N_{py} axis). Light grey = carbon, red = oxygen, orange = phosphorus, dark grey = platinum. For clarity PMe_3 instead of PEt_3 has been used and hydrogens are omitted.

To further study the dynamic behaviour, the largest heteroleptic molecular rectangle **3** was probed between 30 °C to −80 °C using variable temperature NMR (VT-NMR) spectroscopy in CD_2Cl_2, specifically monitoring the relevant aromatic region. The two doublets at δ 8.47 and 8.13 ppm significantly shift downfield to δ 8.70 ppm, close to the shift observed for the free ligand (δ 8.82 ppm) (Figure 4). Moreover, the decrease in temperature only has a minimal effect on the shifts of all other signals, indicating that the observed downfield shift for the PBI-hydrogens is at least partly innate to the system and not solely related to temperature. The original spectrum with two clearly separated doublets is regenerated upon reheating an NMR-sample of **3** to room temperature, demonstrating its stability. For comparison, the VT NMR spectra of **1** over the same temperature range showed a linear downfield shift for both doublets with temperature of only about 0.1 ppm (see

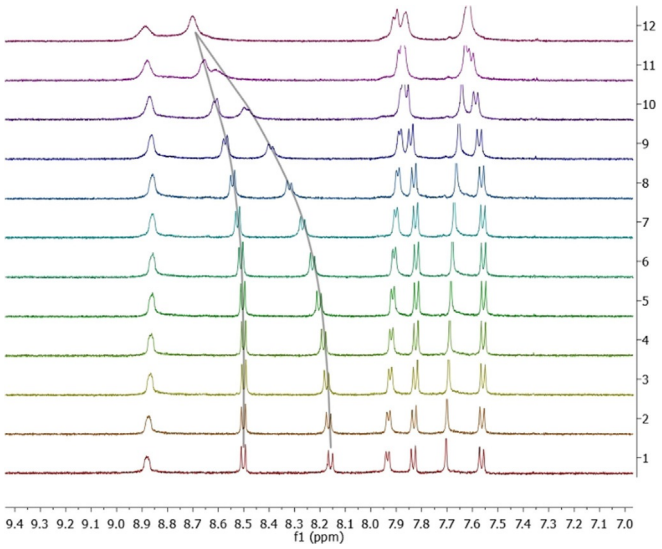

Figure 4. VT ^{1}H NMR spectra of **3** in CD_2Cl_2 from 30 °C (bottom) to −80 °C (top), including trendlines (black) to illustrate coalescence for two bay hydrogens H_A and H_B observed at low temperature.

Supporting Information). These observations show that the smaller assembly is minimally affected by the decrease in temperature as a result of the already close-packed PBI-motifs. The observed coalescence at low temperature is suggestive of a rotating movement rather than the twisting motion observed in Würthner's cyclophane system. Molecular modelling data suggest that both conformations of the rectangle structure, that is, i) two PBI-ligands in "parallel" orientation and ii) PBI-ligands in a "rotated perpendicular" conformation, co-exist at r.t., with the former being energetically favoured. According to the VT NMR spectroscopic data, these systems are in rapid exchange, as a single set of signals is observed. The two sharp doublets observed are a result of the difference in shielding of the aromatic protons upon rotation of one PBI ring toward the aromatic surface of the second PBI ring, whereas these protons have the same chemical shift in the free building block. At lower temperature, the equilibrium between the two conformations is shifted to the more stable "parallel" form, resulting in the gradual disappearance of the contribution of the "rotated" conformer to these aromatic signals. Broadening of the signals may also indicate a change from rapid to slow exchange on the NMR time scale (as observed for **PBI-pyr$_2$** and **1**), associated with coalescence at even lower T.

Electrochemistry of Empty 1–3

Redox-active perylene bisimides are capable of reversibly accepting two electrons at mild potentials. Cyclic voltammetry (CV) was used to determine i) to what extent the redox-properties of the free **PBI-Pyr$_2$** ligand (Figure 5, blue line), are conserved in the heteroleptic rectangle **1** (Figure 5, black line), ii) whether there is any notable influence of the proximity of two PBI-motifs and iii) if the pyrene guest has an influence on the redox-active properties of the assembly. At first glance, the cyclic voltammograms of both free **PBI-Pyr$_2$** ligand and **1** in di-

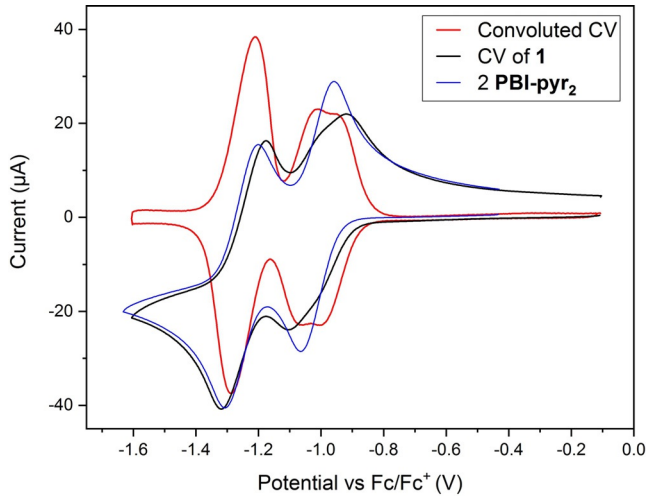

Figure 5. Cyclic voltammogram of **1** (black) and free **PBI-Pyr$_2$** (blue; **[PBI-Pyr$_2$]** = 2x[**1**] used) in CH_2Cl_2 (scan rate of 200 mV s^{-1}, referenced to Fc/Fc$^+$) as well as convoluted cyclic voltammogram for **1** (red).

chloromethane[25] showed two reduction events ($E^1_{1/2} = -1.05$ V, $E^2_{1/2} = -1.3$ V), assigned to the PBI→PBI$^{-\cdot}$ and PBI$^{-\cdot}$→PBI^{2-} redox couples, respectively.[26] Assuming that these events occur simultaneously in both PBI-fragments present in assembly **1**, these redox events involve transfer (or storage) of four electrons, going from parent [Pt$_4$(**PBI-Pyr$_2$**)$_2$L′$_2$]$^{4+}$ via [Pt$_4$(**PBI$^{-\cdot}$-Pyr$_2$**)$_2$L′$_2$]$^{2+}$ to the neutral [Pt$_4$(**PBI^{2-}-Pyr$_2$**)$_2$L′$_2$]^0 complex. However, closer inspection revealed that the first reduction wave for **1** and its corresponding re-oxidation wave are both best described as a combination of two separate events that are split by 60 mV. This is most clearly seen after convolution of the original CV spectrum (Figure 5).

Rectangles **2** and **3** also undergo two fully reversible reduction and re-oxidation events of the PBI-motifs in CH_2Cl_2. Surprisingly, whereas **1** only showed minor splitting of the first redox-wave (Δ60 mV), significant peak potential differences are observed for the rectangles based on **np** (Δ192 mV) and **bp** (Δ239 mV). Deconvolution of the individual waves reveals that in both cases the ratio between the first event (at $E_{1/2} = -0.86$ V for **2**, $E_{1/2} = -0.83$ V for **3**) and the subsequent two events is 1:1:2 in surface area (Figure 6 and Figure 7). Firstly, this confirms overall four-electron processes in both cases, refuting the possibility of a new redox-event occurring with these two systems. Secondly, this suggests that the first redox event relates to a single-electron transfer process, going from [Pt$_4$(**PBI-Pyr$_2$**)$_2$L′$_2$]$^{4+}$ to a ligand mixed-valent[27] [Pt$_4$(**PBI-Pyr$_2$**)(**PBI$^{-\cdot}$-Pyr$_2$**)L′$_2$]$^{3+}$ complex, containing one non-reduced PBI-unit and one mono-reduced PBI-unit. Thereafter, a second single-electron process reduces this species ($E_{1/2} = -1.07$ V for **2**, $E_{1/2} = -1.08$ V for **3**) to [Pt$_4$(**PBI$^{-\cdot}$-Pyr$_2$**)$_2$L′$_2$]$^{2+}$, which is quickly followed by a two-electron reduction to the fully reduced, neutral [Pt$_4$(**PBI^{2-}-Pyr$_2$**)$_2$L′$_2$]^0 complex.

When comparing the convoluted cyclic voltammograms of all three heteroleptic assemblies, a clear correlation between the first overall two-electron reduction with spacer length is observed, with increased size leading to larger splitting into

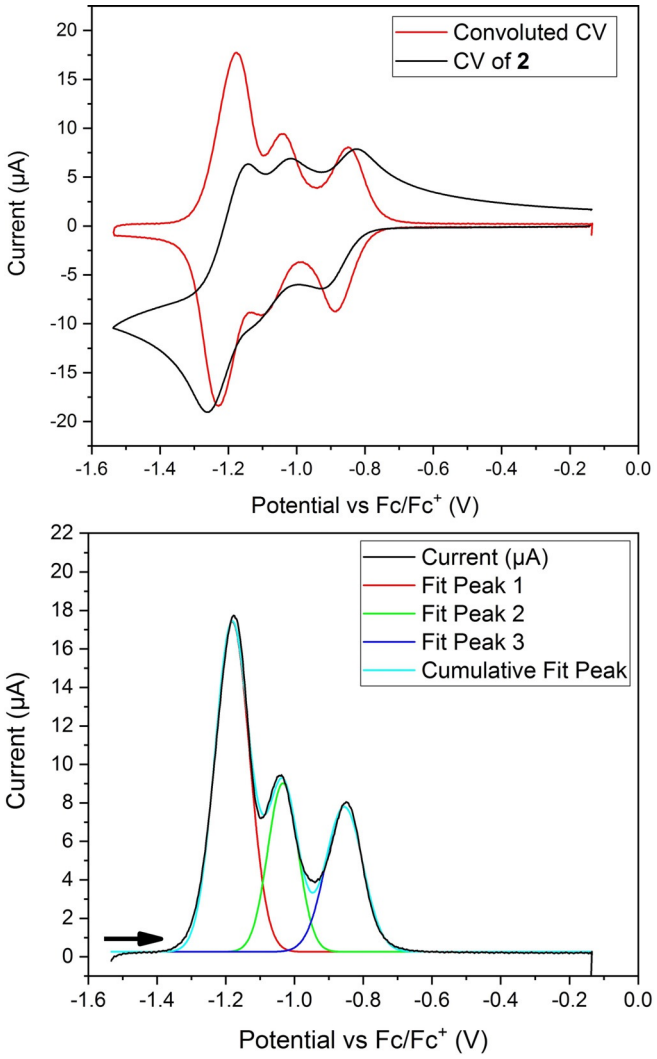

Figure 6. Top: Cyclic voltammetry and convoluted CV of **2** in CH_2Cl_2 with a scan speed of 200 mV s^{-1}, referenced to Fc/Fc$^+$. Bottom: Deconvolution analysis of the re-oxidation events using Gaussian curves, displaying a surface area ratio of 2:1:1 for the different redox events, going from left to right. Arrow indicates scanning direction.

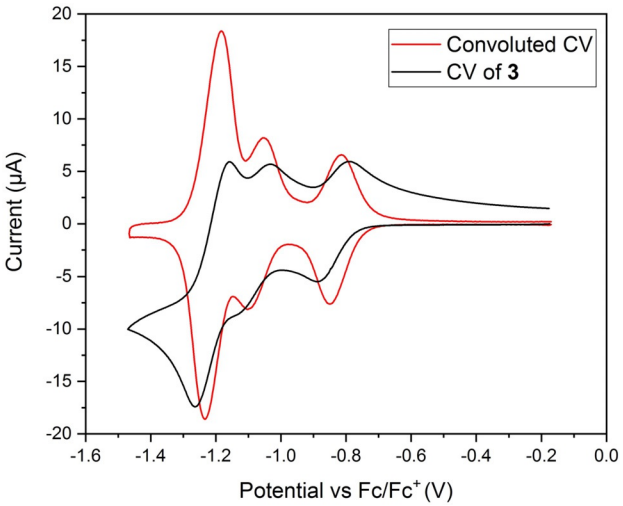

Figure 7. Cyclic voltammetry and convoluted CV of **3** in CH_2Cl_2 with a scan speed of 200 mV s^{-1}, referenced to Fc/Fc$^+$. See Figure S13 for a deconvolution analysis of the re-oxidation events.

two single-electron events (Figure 8). Contrastingly, the second two-electron reduction at $E_{1/2} = -1.20$ V appears independent of spacer length. The observed correlation between redox-event splitting with increased cage size seems counter-intuitive, as an increased intramolecular PBI-PBI distance should lead to decreased electronic communication and repulsion upon reduction. However, as determined by NMR spectroscopy (vide supra), a large intramolecular distance between both aromatic systems induces more rotational freedom in the overall system, whereas the smallest rectangle based on terephthalate linkers confines both PBI units to a near-stacking geometry. Hence, rotation may induce chemical inequivalence of the two PBI units or increase chemical communication, inducing an electronic dependency in the reduction of both fragments.

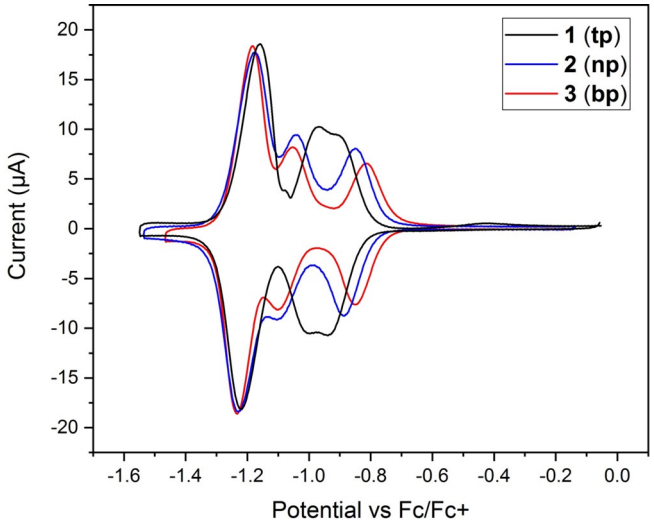

Figure 8. Comparison of convoluted cyclic voltammograms of **1** (black), **2** (blue) and **3** (red) in CH_2Cl_2 with a scan speed of 200 mV s^{-1}.

Electrochemistry of heteroleptic molecular rectangle 1 in the presence of pyrene

To probe the effect of a guest molecule on the redox-properties of the host, the cyclic voltammetry of **1** was measured in the presence of pyrene in MeCN. Host **1** showed an appreciable binding interaction with this guest, as evidenced by the NMR experiments. Stepwise addition of pyrene (between 0–30 equiv) to a solution of **1** in MeCN (at 1 mM concentration, that is, four times as high as used for the NMR-based binding study; see Supporting Information for details) whilst measuring the CV after each addition led to the data displayed in Figure 9. The peak potentials of the two one-electron reduction events ($E^1_{1/2} = -0.9$ V, $E^2_{1/2} = -1.1$ V) clearly shift closer together with higher guest loading. The first event displays a maximum anodic shift of 46 mV while the second event shifts cathodically by up to 47 mV. Shifting concurs with pyrene binding, with 92% occupancy reached after addition of 18 equivalents of pyrene (Figure 10).

Although the CV solution is gradually being diluted by the addition of the pyrene stock solution, the current measured during the re-oxidation event—again observed as a sharp signal—steadily increases, concomitant with a cathodic shift of

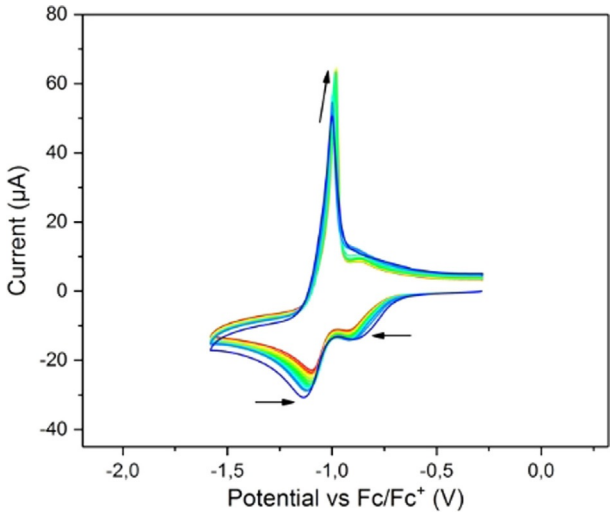

Figure 9. Cyclic voltammograms of **1** in MeCN in the presence of pyrene, going from 0 equivalents (blue) to 30 equivalents (red). Scan speed of 300 mV s^{-1}, referenced to Fc/Fc$^+$.

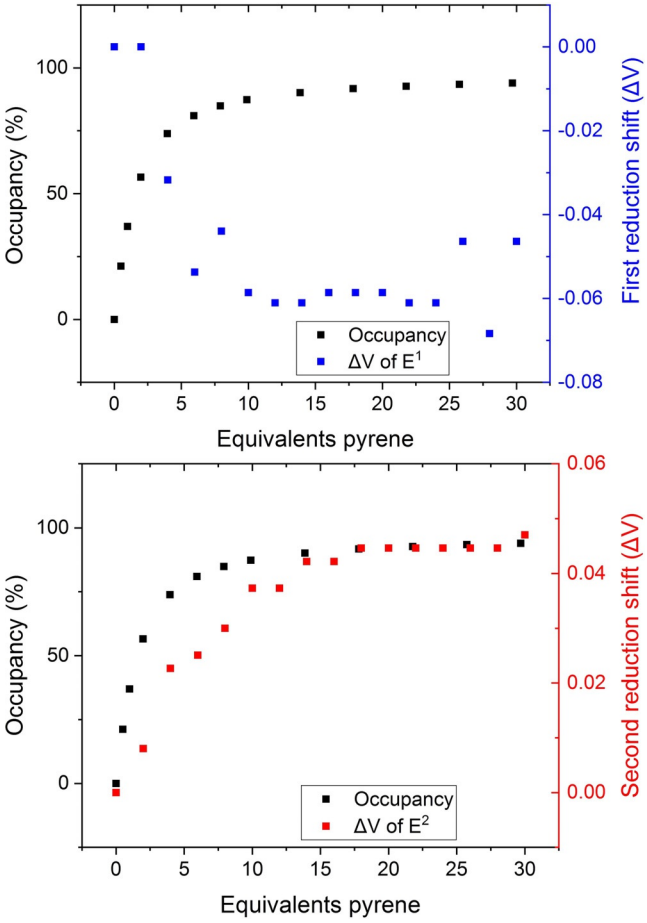

Figure 10. Shifts observed for the peak potential of (top) the first reduction ($E^1_{1/2} = -0.9$ V) and (bottom) the second reduction ($E^2_{1/2} = -1.1$ V) in MeCN. Both plots have the calculated occupancy of pyrene in **1** displayed in black. All data are plotted versus the equivalents of pyrene added to the mixture.

the peak potential. Plotting the peak potential versus the equivalents of pyrene added to the mixture reveals an interesting S-curve instead of an exponential curve anticipated for equimolar host-guest binding (Figure 11). This likely relates to the adsorption of the doubly reduced $\mathbf{1}^{2-}$ onto the electrode, as is also observed in the experiments in absence of pyrene, which affects the encapsulation process (or vice versa). Importantly, the electrochemical experiments clearly illustrate that the redox properties of a supramolecular host can directly be influenced by a guest molecule that binds in the cavity of the assembly.

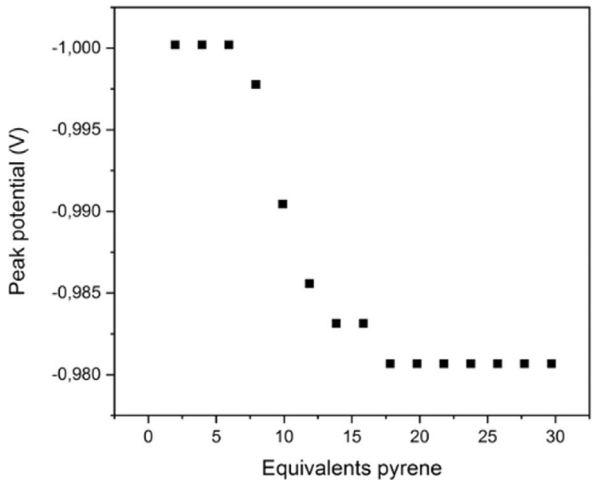

Figure 11. Peak potential of the sharp back oxidation during cyclic voltammetry of **1** in MeCN plotted versus the equivalents pyrene added to the mixture.

Conclusions

Three new heteroleptic $\mathbf{M_4L_2L'_2}$ rectangles **1**–**3**, based on dicarboxylate struts with different size, were synthesized and fully characterized using ^{1}H, ^{13}C, ^{31}P NMR spectroscopy and high-resolution mass spectrometry. Self-assembled system **1** binds pyrene with an association constant of $964 \pm 55\ M^{-1}$, whereas the larger system **3** only shows weak interaction with this small aromatic guest (K_{assoc} of $48 \pm 2\ M^{-1}$). The higher binding in **1** is a result of the close proximity of the PBI-fragments that allows ditopic binding, that is, sufficient π-π interactions between the aromatic guest and both PBI units of the host.

Probing the redox-properties of **1**–**3** by cyclic voltammetry revealed that each PBI-fragment in the assembly can be reversibly reduced by two electrons, resulting in the overall injection of four electrons into these supramolecular heteroleptic assemblies. Cyclic voltammetry in CH_2Cl_2 reveals spacer length-dependent splitting of the first reduction event, converting this overall two-electron process into two single-electron processes. Upon moving from the shortest strut **tp** via **np** to **bp**, the observed peak potential difference between both one-electron processes is 60, 192 and 239 mV, respectively. This increase in electronic communication in assemblies in which the distance between PBI-fragments is larger can be explained by rotational freedom of the **PBI-pyr$_2$** ligand over its longitudinal axis, leading to interactions between the two units. In line with this, the ^{1}H NMR spectra show upfield shifting and splitting of the PBI-hydrogens as a result of the intramolecular PBI-PBI interactions, which is larger for the larger rectangles.

Electrochemical experiments with **1** in the presence of pyrene as guest show that the reduction potentials are influenced by the binding event, which may provide a basis for electronic sensing applications. In addition, the binding properties of these assemblies may be redox-tunable, which eventually could lead to switchable host-guest chemistry.

Acknowledgements

This work has been funded by NWO Chemical Sciences TOP-PUNT Grant 'Catalysis in Confined Spaces' 718.015.004. We thank Ed Zuidinga and Eduard O. Bobylev for assistance with mass spectrometry and Jan-Meine Ernsting and Andreas W. Ehlers for assistance with NMR spectroscopy. Open access funding enabled and organized by Projekt DEAL.

Conflict of interest

The authors declare no conflict of interest.

Keywords: electrochemical sensing · host-guest chemistry · perylene bisimides · redox-active ligand · supramolecular assemblies

[1] R. V. Slone, J. T. Hupp, *Inorg. Chem.* **1997**, *36*, 5422 – 5423.
[2] F. Würthner, A. Sautter, D. Schmid, P. J. A. Weber, *Chem. Eur. J.* **2001**, *7*, 894 – 902.
[3] M. Fujita, J. Yazaki, K. Ogura, *J. Am. Chem. Soc.* **1990**, *112*, 5645 – 5647.
[4] S. Krishnaswamy, S. Prusty, D. Chartrand, G. S. Hanan, D. K. Chand, *Cryst. Growth Des.* **2018**, *18*, 2016 – 2030.
[5] D. Liu, Y.-J. Lin, F. Aznarez, G.-X. Jin, *Cryst. Growth Des.* **2018**, *18*, 6911 – 6917.
[6] B. Therrien, *Eur. J. Inorg. Chem.* **2009**, 2445 – 2453.
[7] A. N. Oldacre, A. E. Friedman, T. R. Cook, *J. Am. Chem. Soc.* **2017**, *139*, 1424 – 1427.
[8] X. Chang, Z. Zhou, C. Shang, G. Wang, Z. Wang, Y. Qi, Z.-Y. Li, H. Wang, L. Cao, X. Li, Y. Fang, P. J. Stang, *J. Am. Chem. Soc.* **2019**, *141*, 1757 – 1765.
[9] G. Gupta, A. Das, S. Panja, J. Y. Ryu, J. Lee, N. Mandal, C. Y. Lee, *Chem. Eur. J.* **2017**, *23*, 17199 – 17203.
[10] a) Z. Li, X. Yan, F. Huang, H. Sepehrpour, P. J. Stang, *Org. Lett.* **2017**, *19*, 5728 – 5731; b) T. R. Cook, P. J. Stang, *Chem. Rev.* **2015**, *115*, 7001 – 7045; c) R. Chakrabarty, P. S. Mukherjee, P. J. Stang, *Chem. Rev.* **2011**, *111*, 6810 – 6918.
[11] a) R. F. Winter, *Curr. Opin. Electrochem.* **2018**, *8*, 14 – 23; b) A. Jana, S. Bähring, M. Ishida, S. Goeb, D. Canevet, M. Sallé, J. O. Jeppesen, J. L. Sessler, *Chem. Soc. Rev.* **2018**, *47*, 5614 – 5645; c) T. Y. Kim, R. A. S. Vasdev, D. Preston, J. D. Crowley, *Chem. Eur. J.* **2018**, *24*, 14878 – 14890; d) W. Wang, Y.-X. Wang, H.-B. Yang, *Chem. Soc. Rev.* **2016**, *45*, 2656 – 2693; e) L. Xu, Y.-X. Wang, L.-J. Chen, H.-B. Yang, *Chem. Soc. Rev.* **2015**, *44*, 2148 – 2167; f) V. Croué, S. Goeb, M. Sallé, *Chem. Commun.* **2015**, *51*, 7275 – 7289; g) A. J. McConnell, C. S. Wood, P. P. Neelakandan, J. R. Nitschke, *Chem. Rev.* **2015**, *115*, 7729 – 7793; h) "Structural Transformations in Coordination Cages": M. D. Johnstone, G. H. Clever in *Comprehensive Supramolecular Chemistry II* (Ed.: J. L. Atwood), Elsevier, London, **2017**.
[12] Recent progress in the design of (mainly 3D) redox-active assemblies: a) S. Krykun, M. Dekhtiarenko, D. Canevet, V. Carré, F. Aubriet, E. Levillain, M. Allain, Z. Voitenko, M. Sallé, S. Goeb, *Angew. Chem. Int. Ed.* **2020**,

59, 716 – 720; *Angew. Chem.* **2020**, *132*, 726 – 730;b) Z. Lu, T. K. Ronson, J. R. Nitschke, *Chem. Sci.* **2020**, *11*, 1097 – 1101; c) F. Jia, H. V. Schröder, L.-P. Yang, C. von Essen, S. Sobottka, B. Sarkar, K. Rissanen, W. Jiang, C. A. Schalley, *J. Am. Chem. Soc.* **2020**, *142*, 3306 – 3310; d) Z. Lu, R. Lavendomme, O. Burghaus, J. R. Nitschke, *Angew. Chem. Int. Ed.* **2019**, *58*, 9073 – 9077; *Angew. Chem.* **2019**, *131*, 9171 – 9175; e) Y. Satoh, L. Catti, M. Akita, M. Yoshizawa, *J. Am. Chem. Soc.* **2019**, *141*, 12268 – 12273; f) G. Szalóki, V. Croué, V. Carré, F. Aubriet, O. Alévêque, E. Levillain, M. Allain, J. Aragó, E. Ortí, S. Goeb, M. Sallé, *Angew. Chem. Int. Ed.* **2017**, *56*, 16272 – 16276; *Angew. Chem.* **2017**, *129*, 16490 – 16494; g) K. Yazaki, S. Noda, Y. Tanaka, Y. Sei, M. Akita, M. Yoshizawa, *Angew. Chem. Int. Ed.* **2016**, *55*, 15031 – 15034; *Angew. Chem.* **2016**, *128*, 15255 – 15258; h) V. Croué, S. Goeb, G. Szalóki, M. Allain, M. Sallé, *Angew. Chem. Int. Ed.* **2016**, *55*, 1746 – 1750; *Angew. Chem.* **2016**, *128*, 1778 – 1782; i) T. Ogoshi, T. Akutsu, Y. Shimada, T. Yamagishi, *Chem. Commun.* **2016**, *52*, 6479 – 6481; j) K. Mahata, P. D. Frischmann, F. Würthner, *J. Am. Chem. Soc.* **2013**, *135*, 15656 – 15661.

[13] R. Plessius, N. Orth, I. Ivanović-Burmazović, M. A. Siegler, J. N. H. Reek, J. I. van der Vlugt, *Chem. Commun.* **2019**, *55*, 12619 – 12622.

[14] F. Würthner, C. R. Saha-Möller, B. Fimmel, S. Ogi, P. Leowanawat, D. Schmidt, *Chem. Rev.* **2016**, *116*, 962 – 1052.

[15] A. Nowak-Król, F. Würthner, *Org. Chem. Front.* **2019**, *6*, 1272 – 1318.

[16] a) P. Spenst, A. Sieblist, F. Würthner, *Chem. Eur. J.* **2017**, *23*, 1667 – 1675; b) P. Spenst, F. Würthner, *J. Photochem. Photobiol. C* **2017**, *31*, 114 – 138.

[17] Recent examples of redox-active molecular assemblies: a) K. Herasymchuk, J. J. Miller, G. A. MacNeil, A. S. Sergeenko, D. McKearney, S. Goeb, M. Sallé, D. B. Leznoff, T. Storr, *Chem. Commun.* **2019**, *55*, 6082 – 6085; b) J.-Y. Balandier, M. Chas, S. Goeb, P. I. Dron, D. Rondeau, A. Belyasmine, N. Gallego, M. Sallé, *New J. Chem.* **2011**, *35*, 165 – 168.

[18] C. Addicott, I. Oesterling, T. Yamamoto, K. Müllen, P. J. Stang, *J. Org. Chem.* **2005**, *70*, 797 – 801.

[19] For an alternative strategy to tune the inner cavity of heteroleptic assemblies (varying the bispyridine strut), see: N. P. E. Barry, J. Furrer, J. Freudenreich, G. Süss-Fink, B. Therrien, *Eur. J. Inorg. Chem.* **2010**, 725 – 728.

[20] P. D. Frischmann, F. Würthner, *Org. Lett.* **2013**, *15*, 4674 – 4677.

[21] Y. Zheng, Z. Zhao, M. Wang, K. Ghosh, J. B. Pollock, T. R. Cook, P. J. Stang, *J. Am. Chem. Soc.* **2010**, *132*, 16873 – 16882.

[22] a) K.-W. Chi, C. Addicott, A. M. Arif, P. J. Stang, *J. Am. Chem. Soc.* **2004**, *126*, 16569 – 16574; b) K.-W. Chi, C. Addicott, M.-E. Moon, H. J. Lee, S. C. Yoon, P. J. Stang, *J. Org. Chem.* **2006**, *71*, 6662 – 6665.

[23] F. Würthner, *Chem. Commun.* **2004**, 1564 – 1579.

[24] F. Schlosser, M. Moos, C. Lambert, F. Würthner, *Adv. Mater.* **2013**, *25*, 410 – 414.

[25] In acetonitrile, adsorption of the neutral $[Pt_4(PBI^{2-}\text{-}Pyr_2)_2L'_2]^0$ complex onto the electrode was observed (see Figure S12), which complicated analysis of the re-oxidation event.

[26] These potentials are very similar to those observed for a homoleptic Pt_4 square containing a slightly shorter **PBI-Pyr$_2$** variant: F. Würthner, A. Sautter, *Chem. Commun.* **2000**, 445 – 446. This supports PBI-centered redox regardless of and without further redox occurring on the dicarboxylate spacer employed.

[27] For recent other ligand mixed-valent systems from our group, see: a) D. L. J. Broere, L. L. Metz, B. de Bruin, J. N. H. Reek, M. A. Siegler, J. I. van der Vlugt, *Angew. Chem. Int. Ed.* **2015**, *54*, 1516 – 1520; *Angew. Chem.* **2015**, *127*, 1536 – 1540; b) D. L. J. Broere, R. Plessius, J. Tory, S. Demeshko, B. de Bruin, M. A. Siegler, F. Hartl, J. I. van der Vlugt, *Chem. Eur. J.* **2016**, *22*, 13965 – 13975; c) D. L. J. Broere, D. K. Modder, E. Blokker, M. A. Siegler, J. I. van der Vlugt, *Angew. Chem. Int. Ed.* **2016**, *55*, 2406 – 2410; *Angew. Chem.* **2016**, *128*, 2452 – 2456.

Manuscript received: March 22, 2020
Revised manuscript received: April 28, 2020
Accepted manuscript online: May 19, 2020
Version of record online: September 21, 2020